Research Article

Nano Research
2022, 15(1): 304–309

ISSN 1998-0124 CN 11-5974/O4
https://doi.org/10.1007/s12274-021-3474-0

N-doped carbon nanotubes supported $CoSe_2$ nanoparticles: A highly efficient and stable catalyst for H_2O_2 electrosynthesis in acidic media

Longcheng Zhang[1,2,§], Jie Liang[2,§], Luchao Yue[1,2], Zhaoquan Xu[2], Kai Dong[2], Qian Liu[2], Yonglan Luo[2], Tingshuai Li[2], Xiaohong Cheng[3] (✉), Guanwei Cui[4], Bo Tang[4], Abdulmohsen Ali Alshehri[5], Khalid Ahmed Alzahrani[5], Xiaodong Guo[1] (✉), and Xuping Sun[2] (✉)

[1] *School of Chemical Engineering, Sichuan University, Chengdu 610065, China*
[2] *Institute of Fundamental and Frontier Sciences, University of Electronic Science and Technology of China, Chengdu 610054, China*
[3] *Hubei Key Laboratory of Low Dimensional Optoelectronic Materials and Devices, Hubei University of Arts and Science, Xiangyang 441053, China*
[4] *College of Chemistry, Chemical Engineering and Materials Science, Shandong Normal University, Jinan 250014, China*
[5] *Chemistry Department, Faculty of Science & Center of Excellence for Advanced Materials Research, King Abdulaziz University, P.O. Box 80203, Jeddah, 21589, Saudi Arabia*
[§] *Longcheng Zhang and Jie Liang contributed equally to this work.*

Received: 24 February 2021 / **Revised:** 24 March 2021 / **Accepted:** 25 March 2021

ABSTRACT

Electrocatalytic oxygen reduction reaction (ORR) provides an attractive alternative to anthraquinone process for H_2O_2 synthesis. Rational design of earth-abundant electrocatalysts for H_2O_2 synthesis via a two-electron ORR process in acids is attractive but still very challenging. In this work, we report that nitrogen-doped carbon nanotubes as a multi-functional support for $CoSe_2$ nanoparticles not only keep $CoSe_2$ nanoparticles well dispersed but alter the crystal structure, which in turn improves the overall catalytic behaviors and thereby renders high O_2-to-H_2O_2 conversion efficiency. In 0.1 M $HClO_4$, such $CoSe_2$@NCNTs hybrid delivers a high H_2O_2 selectivity of 93.2% and a large H_2O_2 yield rate of 172 ppm·h^{-1} with excellent durability up to 24 h. Moreover, $CoSe_2$@NCNTs performs effectively for organic dye degradation via electro-Fenton process.

KEYWORDS

cobalt selenide, nitrogen-doped carbon nanotube, electrocatalysis, two-electron oxygen reduction reaction, hydrogen peroxide

1 Introduction

As a strong and clean oxidant, H_2O_2 has widespread industrial applications [1–3], and it is recently used as a disinfectant during the COVID-19 pandemic as well [4]. However, today's increasing market demand and environmental issues necessitate green and energy-saving alternatives to traditional anthraquinone process (safety hazards, substantial byproducts, and energy-intensive purification procedures) for H_2O_2 production [5–8]. Electrocatalytic O_2 reduction reaction (ORR) can convert O_2 to H_2O_2 with simplicity and low environmental impact, while its practical applications need efficient catalyst to improve selectivity toward H_2O_2 product via two-electron ORR (2e$^-$ ORR) and boost the reaction kinetics [9–24]. Encouragingly, efficient H_2O_2 electrosynthesis is achieved with a series of catalysts, most of which operate under alkaline conditions [16–21]. Producing H_2O_2 in acids is equally important because: (i) H_2O_2 can rapidly self-decompose in alkaline media [25]; (ii) anion exchange membrane in practical application is not mature [2]; (iii) H_2O_2 in acid solution is more applicable to applications such as electro-Fenton process [26]. Thus, it is of great significance to design and develop catalysts working efficiently in acids.

In general, noble-metal based catalysts remain the most active for acidic 2e$^-$ ORR [27–29], but the scarcity impedes the widespread use. Transition metal chalcogenides featuring with tunable electronic and crystal structures [30–32] have attracted increasing attention in the field of 2e$^-$ ORR [33–36]. Recent study from Jin's group shows that $CoSe_2$ is efficient to catalyze the 2e$^-$ ORR [35]. Interestingly, it suggests that orthorhombic $CoSe_2$ shows superior activity over its cubic counterpart and the crystal structures can be tuned by varying the annealing temperatures for catalyst preparation. It is well-established that nanocarbon can act as a good material to not only support and stabilize electrocatalysts but enhance their electronic conductivity [37]. We thus believe that $CoSe_2$-carbon nanohybrid would be an attractive electrocatalyst toward more efficient H_2O_2 electrosynthesis, which however has not been explored before.

Here, we report on the development of $CoSe_2$ nanoparticles decorated nitrogen-doped carbon nanotubes ($CoSe_2$@NCNTs) as a superb 2e$^-$ ORR electrocatalyst. NCNTs change the crystal structures of $CoSe_2$ from orthorhombic to cubic phase. In

Address correspondence to Xiaohong Cheng, chengxiaohong0807@126.com; Xiaodong Guo, xiaodong2009@scu.edu.cn; Xuping Sun, xpsun@uestc.edu.cn

0.1 M $HClO_4$, such $CoSe_2$@NCNTs hybrid with near-zero overpotential attains a high selectivity of 93.2% and excellent durability up to 24 h, surpassing its pure $CoSe_2$ counterpart. Moreover, it enables a large H_2O_2 yield rate of up to 172 ppm·h^{-1} as well as an effective electro-Fenton process.

2 Experimental

2.1 Materials

Cobaltous nitrate hexahydrate ($Co(NO_3)_2·6H_2O$), zinc nitrate hexahydrate ($Zn(NO_3)_2·6H_2O$), melamine, selenium (Se) powder, cerium sulfate ($Ce(SO_4)_2$), sodium sulfate ($Na(SO_4)_2$), and iron sulfate heptahydrate ($Fe(SO_4)_2·7H_2O$) were bought from Aladdin Ltd. Nafion (5 wt.%) solution was purchased from Sigma-Aldrich Chemical Reagent Co., Ltd. Anhydrous ethanol, isopropyl alcohol (IPA), potassium nitrate (KNO_3), potassium ferricyanide ($K_3[Fe(CN)_6]$), rhodamine B (RhB), and perchloric acid ($HClO_4$) were purchased from Beijing Chemical Corporation. Ultrapure water (18.25 Ω) use throughout all experiments was purified through a Millipore system. All chemicals were used without further purification.

2.2 Preparation of $CoSe_2$@NCNTs and pure $CoSe_2$

2.102 g of melamine, 1.78 g of $Zn(NO_3)_2·6H_2O$, and 0.291 g of $Co(NO_3)_2·6H_2O$ were added into an appropriate amount of ethanol, which was ground in a mortar for at least 45 min. The mixture was dried at 60 °C for 3 h. Co@NCNTs hybrid was obtained by pyrolysis of above mixture at 800 °C for 2 h under N_2 atmosphere with a heating rate of 5 °C·min^{-1} in a tubular furnace. Subsequently, two ceramic boats containing Se powders and Co@NCNTs powders were placed in the upstream and downstream of the tubular furnace, respectively. Under Ar atmosphere, the samples were heated to 400 °C for 2 h with a heating rate of 2 °C·min^{-1}. The product obtained was denoted as $CoSe_2$@NCNTs. For preparing pure $CoSe_2$, the same fabrication procedure for $CoSe_2$@NCNTs was performed but without using $Zn(NO_3)_2·6H_2O$ and melamine.

2.3 Characterization

X-ray diffraction (XRD) data were acquired on a Shimadzu XRD-6100 diffractometer with Cu Kα radiation (40 kV, 30 mA) of wavelength 0.154 nm. Scanning electron microscopy (SEM) and energy dispersive X-ray (EDX) elemental mapping images were collected on a Gemini SEM 300 scanning electron microscope (ZEISS, Germany) at an accelerating voltage of 5 kV. X-ray photoelectron spectroscopy (XPS) measurements were performed on an ESCALABMK II X-ray photoelectron spectrometer using Mg as the exciting source. Transmission electron microscopy (TEM) images were obtained from a Zeiss Libra 200FE transmission electron microscope operated at 200 kV. Absorbance data were acquired on SHIMADZU UV-2700 Ultraviolet-visible (UV-Vis) spectrophotometer.

2.4 Electrochemical measurements

Electrochemical tests in this work were performed in an aqueous electrolyte of 0.1 M $HClO_4$ with pH value of 1. The formation of H_2O_2 enabled by the active catalysts was studied by using rotating ring disk electrode (RRDE) measurements with a three-electrode system (Ag/AgCl reference electrode and Pt wire counter electrode) under ambient conditions. CHI 760E (CH Instruments, Inc., Shanghai) was used as working station. The ink was prepared by mixing 5 mg of $CoSe_2$@NCNTs catalyst, 730 μL of isopropyl alcohol, 200 μL of H_2O, and 30 μL of Nafion and ultra-sonicating for 1–2 h. Catalyst coated RRDEs (ring area: 0.1866 cm^2, disk area: 0.2475 cm^2) were prepared by dropping or spin-coating (100 rpm) 5 μL of the catalyst ink onto glassy carbon disk, which was dried at room temperatures prior to use. Note that the recorded current density was normalized to the geometric surface area. Before the linear sweep voltammetry (LSV) tests, cyclic voltammetry (CV) was performed in the potential range from 0 to 0.8 V vs. reversible hydrogen electrode (RHE) in Ar-saturated 0.1 M $HClO_4$ electrolyte at 100 mV·s^{-1} for around 50 cycles, in which a steady CV response was obtained. The electrochemical cleaning of Pt ring was then conducted in the same potential range at 200 mV·s^{-1} for 20 cycles. The collection efficiency is determined as 35%. Electrochemical impedance spectroscopy (EIS) was conducted at 0.5 V vs. RHE from 100 KHz to 0.1 Hz. The H_2O_2 production performances (activity and selectivity) were assessed by LSV scans (scan rate: 50 mV·s^{-1}, RRDE rotating speed: 1,600 rpm) in the potential range of 0.0 to 0.8 V vs. RHE. During the LSV tests, the applied potential to the Pt was held at 1.2 V vs. RHE for H_2O_2 detection. The H_2O_2 selectivity (H_2O_2(%)), and electron transfer number (n) were calculated as follows

$$H_2O_2\ (\%) = 200 \times (I_{Ring}/N)/(I_{Disk} + I_{Ring}/N) \quad (1)$$

$$n = 4|I_{Disk}|/(I_{Disk} + I_{Ring}/N) \quad (2)$$

where I_{Ring} is the ring current, I_{Disk} is the disk current.

H_2O_2 produced via bulk ORR electrolysis can be accumulated and quantified during the bulk ORR electrolysis in 0.1 M $HClO_4$. The direct electrosynthesis of H_2O_2 and quantification of H_2O_2 concentration were carried out in a gas-tight H-cell system. The $CoSe_2$@NCNTs (loading 0.1 mg) on a carbon paper electrode (1 cm × 0.5 cm) was prepared as the cathode electrode ($CoSe_2$@NCNTs/CP). A Nafion 117 membrane was employed to separate the chambers. The membrane was protonated by first treating in H_2O_2 aqueous solution (5 wt.%) at 80 °C for 1 h, then washed with deionized water until the pH value of the water returned to normal. Finally, the membranes were soaked with deionized water for 4 h. The electrochemical experiments were carried out with an electrochemical workstation (CHI 760E) using a three-electrode configuration with prepared $CoSe_2$@NCNTs/CP electrode, Pt mesh electrode, and Ag/AgCl electrode as the working electrode, the counter electrode, and the reference electrode, respectively.

2.5 Quantitative detection of H_2O_2

H_2O_2 yield was measured by using the indicator of $Ce(SO_4)_2$ ($2Ce^{4+} + H_2O_2 \rightarrow 2Ce^{3+} + 2H^+ + O_2$). Samples (20 μL tested electrolyte) were collected at a certain time (1 h) and mixed with the $Ce(SO_4)_2$ solution (0.1 mmol·L^{-1}, 3.98 mL). The generated solution was detected with UV-Vis spectrophotometer. A typical concentration-absorbance curve was calibrated by linear fitting the absorbance values at wavelength length of 320 nm for various known concentrations of 0.02, 0.04, 0.06, 0.08, and 0.1 mM of Ce^{4+}. The fitting curve ($y = 4.6883x - 0.00608$, $R^2 = 0.9999$) shows good linear relation of absorbance value with H_2O_2 concentration. The yield of H_2O_2 was finally determined based on the reduced Ce^{4+} concentration.

2.6 Quantitative detection of rhodamine B

Electro-Fenton degradation of Rhodamine B was tested in an H-cell with 30 mL electrolyte of 40 mg·L^{-1} Rhodamine B, 0.5 M $Na_2(SO_4)$, and 0.5 mM Fe^{2+} (pH = 2.85). $CoSe_2$@NCNTs/CP ($CoSe_2$@NCNTs loading of ~ 1.385 mg, 1 cm × 1 cm carbon paper electrode) is served as the cathode electrode. During the electro-Fenton degradation test, 100 μL electrolyte solution was periodically sampled (5 min) from the cathode electrode

compartment in H-cell, and diluted with 3.0 mL 0.5 M Na_2SO_4 (pH = 2.85). The concentration of organic rhodamine B was determined using UV–Vis spectrophotometry.

3 Results and discussion

Figure S1 in the Electronic Supplementary Material (ESM) shows the XRD pattern for Co@NCNTs with three characteristic peaks at 44.2°, 51.5°, and 75.8° indexed to the (111), (200), and (220) planes of Co (PDF No. 15-0806), respectively. The diffraction peak at 25.8° can be assigned to NCNTs [38]. The SEM image further suggests the formation for Co nanoparticles-NCNTs hybrid (Fig. S2 in the ESM). After selenization, except for the diffraction peak of NCNTs, only peaks for orthorhombic phase $CoSe_2$ (PDF No. 53-0449) are observed (Fig. 1(a)), suggesting the complete conversion of Co into orthorhombic $CoSe_2$. Besides, the morphology is well preserved (Fig. 1(b)). The EDX elemental mapping images show the uniform distribution of C, N, Co and Se elements, as shown in Fig. S3 in the ESM. TEM image (Fig. 1(c)) demonstrates the formation of nanoparticles decorated NCNTs. The high-resolution TEM (HRTEM) image taken from such nanoparticle reveals lattice fringes with an interplanar spacing of 0.192 and 0.292 nm indexed to the (211) and (101) planes of orthorhombic $CoSe_2$, respectively (Fig. 1(d)). For comparison, pure $CoSe_2$ particles were synthesized under otherwise identical conditions used for preparing $CoSe_2$@NCNTs but without using $Zn(NO_3)_2{\cdot}6H_2O$ and melamine. It is worth noting that the absence of NCNTs leads to cubic pyrite-type $CoSe_2$ particles (Fig. 1(a)) with much larger sizes (Fig. S4 in the ESM).

The XPS survey spectrum of $CoSe_2$@NCNTs further reveals the existence of Co, N, C, and Se, as shown in Fig. S5 in the ESM. Figure 2(a) presents the C 1s spectrum, which can be deconvoluted as graphitic sp^2 C (284.60 eV), N-sp^2 C (285.46 eV), and N-sp^3 C (287.50 eV) [38, 39]. Deconvoluted N 1s spectrum (Fig. 2(b)) can be split into four components assigned to different nitrogen electronic environments, including pyridinic-N (398.19 eV), pyrrolic-N (399.02 eV), graphitic-N (400.74 eV), and N-oxide (402.11 eV) [38, 40]. The XPS spectrum in the Co 2p region is shown in Fig. 2(c). The binding energies (BEs) at 778.70 and 793.65 eV correspond to Co $2p_{3/2}$ and Co $2p_{1/2}$, and BEs at 781.40 and 797.10 eV are attributed to surface oxidation of Co species, with two satellite peaks at 786.00 and 802.00 eV [41–43]. The spectrum of Se 3d can be fitted into three contributions, at 54.80, 55.70, and 59.40 eV (Fig. 2(d)),

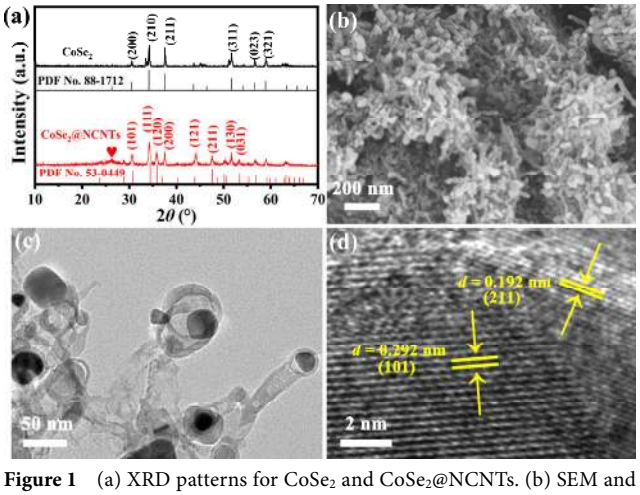

Figure 1 (a) XRD patterns for $CoSe_2$ and $CoSe_2$@NCNTs. (b) SEM and (c) TEM images for $CoSe_2$@NCNTs. (d) HRTEM image taken from one-single $CoSe_2$ nanoparticle.

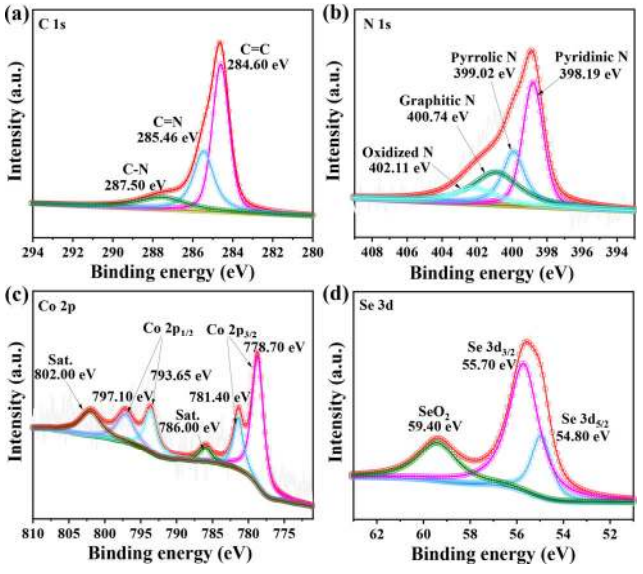

Figure 2 High-resolution (a) C 1s, (b) N 1s, (c) Co 2p, and (d) Se 3d XPS spectra of $CoSe_2$@NCNTs.

which can be ascribed to Se $3d_{5/2}$, Se $3d_{3/2}$, and oxidized Se [44, 45].

The $2e^-$ ORR activity of $CoSe_2$@NCNTs was examined using a RRDE technique. Pure $CoSe_2$ particles and NCNTs were also tested for comparison. All potentials were reported on a RHE scale. Figure 3(a) shows the RRDE voltammograms for $CoSe_2$@NCNTs and pure $CoSe_2$ in 0.1 M $HClO_4$. $CoSe_2$@NCNTs shows larger disk current density and more positive reduction potential (~ 0.68 V for $CoSe_2$@NCNTs and ~ 0.58 V for $CoSe_2$) than $CoSe_2$, suggesting improved reaction kinetics for $CoSe_2$@ NCNTs. Notably, compared with pure $CoSe_2$, $CoSe_2$@NCNTs also offers larger ring current densities (j_{ring}), which is about 1.3 times higher than that of $CoSe_2$ at 0.25 V with an increase of 0.3 $mA{\cdot}cm^{-2}$. Such significant increase in j_{ring} for $CoSe_2$@ NCNTs suggests more efficient O_2-to-H_2O_2 conversion efficiency. As we expected, the NCNTs offers negligible reduction current toward the $2e^-$ ORR (Fig. S6 in the ESM). Moreover, $CoSe_2$@NCNTs shows a decent Tafel slope of only 39.8 $mV{\cdot}dec^{-1}$ (Fig. S7 in the ESM), which is lower than that of $CoSe_2$ (83.8 $mV{\cdot}dec^{-1}$), suggesting $CoSe_2$@NCNTs performs more efficiently toward H_2O_2 electrosynthesis in 0.1 M $HClO_4$. The H_2O_2 selectivity for $CoSe_2$@NCNTs and $CoSe_2$ can then be calculated and is plotted in Fig. 3(b). It is seen that $CoSe_2$@NCNTs displays H_2O_2 selectivity superior to $CoSe_2$ in the potential range of 0–0.4 V and attains the highest selectivity of 93.2% at 0.3 V. Such $CoSe_2$@NCNTs with high selectivity stands out from recent electrocatalysts for acidic $2e^-$ ORR (Fig. 3(c)). The high selectivity for $CoSe_2$@NCNTs is consistent with its electron transfer number (close to 2, Fig. S8 in the ESM) as well, further suggesting a predominant $2e^-$ pathway. The ORR activity of the $CoSe_2$@NCNTs was also evaluated in alkaline media (0.1 M KOH), as shown in Fig. S9 in the ESM. It is observed that $CoSe_2$@NCNTs displays the highest H_2O_2 selectivity of 56% at 0.48 V, which is not as good as those performed in 0.1 M $HClO_4$.

To further understand the effects of introducing NCNTs on the enhanced catalytic performances, more electrochemical measurements were performed. As seen in Fig. S10 in the ESM and Fig. 3(d), the double-layer capacitance (C_{dl}) for $CoSe_2$@NCNTs (1.07 $mF{\cdot}cm^{-2}$) is 11.5 times larger than that of $CoSe_2$ (0.093 $mF{\cdot}cm^{-2}$), revealing much larger electrochemical active surface area, which is beneficial to more efficient O_2

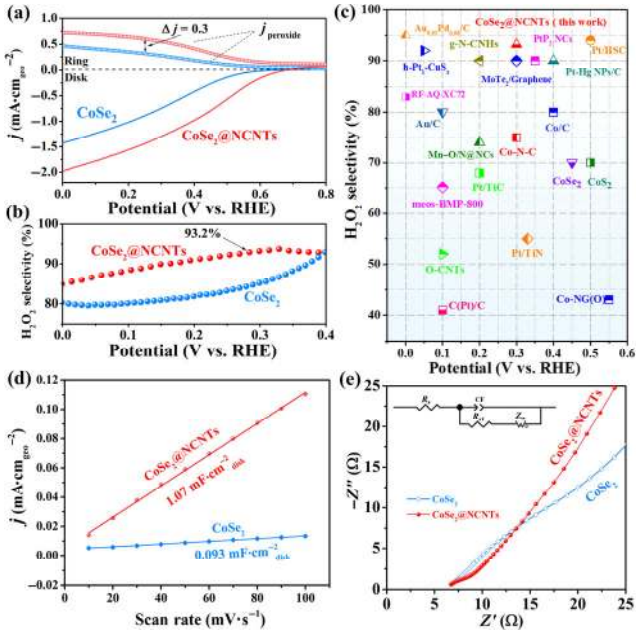

Figure 3 (a) RRDE voltammograms for $CoSe_2$ and $CoSe_2$@NCNTs in 0.1 M $HClO_4$. (b) H_2O_2 selectivity. (c) Selectivity comparison. (d) Capacitive currents as a function of scan rate at 0.806 V vs. RHE and (e) Nyquist plots.

reduction process. EIS measurements further indicate that $CoSe_2$@NCNTs has lower charge transfer resistance than that of $CoSe_2$ (Fig. 3(e)), implying enhanced electronic conductivity for $CoSe_2$ with the presence of NCNTs [46, 47].

In the bulk electrolysis experiment, H_2O_2 concentration after 1 h bulk electrolysis operating at each applied potential (from 0 to 0.2 V) is spectrophotometrically evaluated using a Ce^{4+} titration method. UV–Vis spectra of Ce^{4+} solution with various concentrations (0.02–0.1 mM) and corresponding standard curve (R^2 = 0.9999) are shown in Fig. S11 in the ESM. Inks prepared from $CoSe_2$@NCNTs were deposited dropwise on carbon paper ($CoSe_2$@NCNTs/CP) to serve as the working electrode (catalyst loading of 0.1 mg, geometric area of ~ 0.5 cm^{-2}) in a gas-tight H-cell. The LSV curves for $CoSe_2$ and $CoSe_2$@NCNTs (Fig. S12 in the ESM) show that a nearly 2.5-fold increase in cell current for $CoSe_2$@NCNTs/CP at 0.1 V vs. RHE. As shown in Fig. 4(a), higher current densities can be achieved when the potentials applied to the $CoSe_2$@NCNTs/CP electrode become more negative, which even attains approximately 21 mA·cm^{-2} at 0 V vs. RHE. Meanwhile, the most negative potential also affords the highest H_2O_2 yield rate of 172 ppm·h^{-1} (Fig. 4(b)). Thus, $CoSe_2$@NCNTs is a promising catalyst for mass H_2O_2 production.

To probe the ability of $CoSe_2$@NCNTs/CP for on-site water treatment, rhodamine B (RhB) as a model organic pollutant was used to perform electro-Fenton process over $CoSe_2$@NCNTs/CP. The content of RhB at various time points during the electro-Fenton process in the cathode compartment of an H-cell was detected by spectrophotometer measurement (Fig. S13 in the ESM). Calibration curves and corresponding fitting curves are shown in Figs. S13(a) and S13(b) in the ESM. Current density of the $CoSe_2$@NCNTs/CP in acidified solution (pH = 2.85) is displayed in the Fig. 4(c). As shown in Fig. 4(d), 40 mg·L^{-1} of Rh B can be completely degraded by the $CoSe_2$@NCNTs/CP electrode within a short period of 40 min, suggesting an effective electro-Fenton process. These results not only confirm that the H_2O_2 produced by $CoSe_2$@NCNTs/CP can be accumulated to remove organic pollutants, but show the potential of $CoSe_2$@NCNTs as a catalyst for practical applications such as water treatment.

To assess durability of $CoSe_2$@NCNTs and pure $CoSe_2$ under working conditions, 24 h electrolysis tests were performed at 0.1 V vs. RHE (Fig. 4(e)). As it was supposed, the introduction of NCNTs substantially improves the overall stability with a two-fold increase in current density. Such enhancements highlight the important role of carbon support in boosting the efficiency and stability of the catalytic systems [37, 48]. More specifically, $CoSe_2$@NCNTs only exhibits 9% loss in current density after 24 h electrolysis, whereas the current density of pure $CoSe_2$ shows severe fluctuation with a 91% loss. Impressively, the XRD pattern (Fig. S14 in the ESM) of post-ORR $CoSe_2$@NCNTs was also obtained, which confirmed the good structural stability of $CoSe_2$@NCNTs towards $2e^-$ ORR in 0.1 M $HClO_4$ solution.

It is important to note that the $2e^-$ ORR catalytic performance of $CoSe_2$@NCNTs outperforms its $CoSe_2$ counterpart and many reported catalysts in acidic media (Table S1 in the ESM). And its superior overall performance can be rationally attributed to the following four reasons: (1) crystal structure change

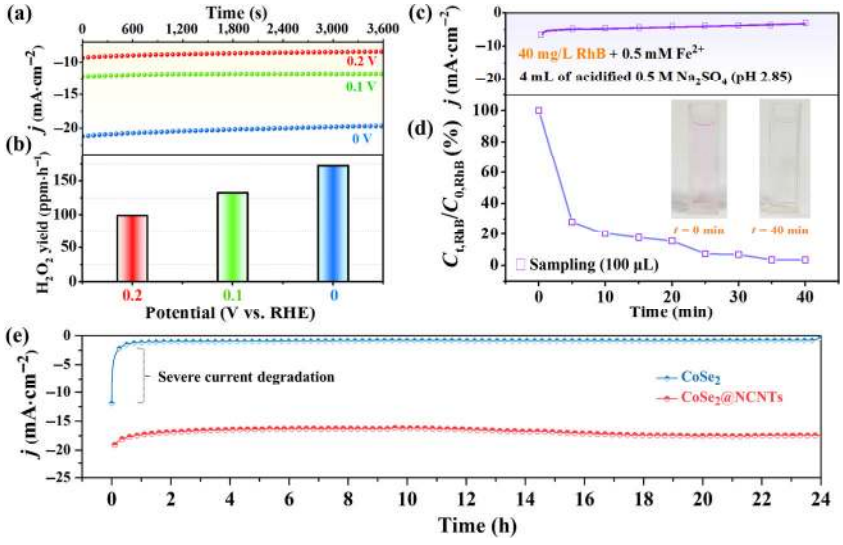

Figure 4 (a) Chronoamperometry curves for $CoSe_2$ and $CoSe_2$@NCNTs under various potentials for 3600 s and (b) corresponding H_2O_2 yields. (c) Chronoamperometry curves of $CoSe_2$@NCNTs at 0.5 V vs. RHE when both RhB and Fe^{2+} are present in O_2-saturated acidified 0.5 M Na_2SO_4 solution (pH 2.85). (d) Decays of the RhB concentrations over time. (e) Long-term stability for $CoSe_2$ and $CoSe_2$@NCNTs at 0.1 V vs. RHE in 0.1 M $HClO_4$ for 24 h.

of $CoSe_2$ caused by NCNTs favors more efficient O_2-to-H_2O_2 conversion process in acids; (2) NCNTs as carbon support can enhance the stability of supported active species further, assuring excellent durability for H_2O_2 electrosynthesis; (3) NCNTs favours the formation of more dispersed nanoparticles with smaller size and thus the exposure of more active sites; (4) NCNTs with the lone-pair electron in N atoms can greatly enhance electronic conductivity and reactivity, leading to more facile electrode kinetics.

4 Conclusions

In summary, $CoSe_2$@NCNTs nanohybrid is proposed as an efficient catalyst for electrocatalytic O_2 reduction to H_2O_2. When tested in 0.1 M $HClO_4$, it attains a high H_2O_2 selectivity of 93.2% and a large H_2O_2 yield rate of 172 ppm·h^{-1}, with excellent stability for at least 24 h under working conditions. Moreover, this catalyst also exhibits good degradation ability toward organic RhB via effective electro-Fenton process. The present work not only offers a robust low-cost catalyst for efficient H_2O_2 electrosynthesis but would open a new avenue to rationally design metal chalcogenide-carbon nanohybrids toward enhanced $2e^-$ ORR electrocatalysis.

Acknowledgements

This work was supported by the National Natural Science Foundation of China (Nos. 22072015, 21878195 and U20A20145), the Scientific and technological achievement transformation project of Sichuan Science and Technology Department (No. 21ZHSF0111), and Shanghai Scientific and Technological Innovation Project (No. 18JC1410604).

Electronic Supplementary Material: Supplementary material (SEM images, EDX mapping images, XPS spectrum, XRD patterns, RRDE voltammogram, Tafel plots, cyclic voltammograms, UV–Vis spectra, and Tables S1) is available in the online version of this article at https://doi.org/10.1007/s12274-021-3474-0.

References

[1] Campos-Martin, J. M.; Blanco-Brieva, G.; Fierro, J. L. G. Hydrogen peroxide synthesis: An outlook beyond the anthraquinone process. *Angew. Chem., Int. Ed.* **2006**, *45*, 6962–6984.

[2] Yang, S.; Verdaguer-Casadevall, A.; Arnarson, L.; Silvioli, L.; Čolić, V.; Frydendal, R.; Rossmeisl, J.; Chorkendorff, I.; Stephens, I. E. L. Toward the decentralized electrochemical production of H_2O_2: A focus on the catalysis. *ACS Catal.* **2018**, *8*, 4064–4081.

[3] Yamada, Y.; Yoneda, M.; Fukuzumi, S. High and robust performance of H_2O_2 fuel cells in the presence of scandium ion. *Energy Environ. Sci.* **2015**, *8*, 1698–1701.

[4] Mahmood, A.; Eqan, M.; Pervez, S.; Alghamdi, H. A.; Tabinda, A. B.; Yasar, A.; Brindhadevi, K.; Pugazhendhi, A. COVID-19 and frequent use of hand sanitizers; human health and environmental hazards by exposure pathways. *Sci. Total Environ.* **2020**, *742*, 140561.

[5] Li, H. B.; Zheng, B.; Pan, Z. Y.; Zong, B. N.; Qiao, M. H. Advances in the slurry reactor technology of the anthraquinone process for H_2O_2 production. *Front. Chem. Sci. Eng.* **2018**, *12*, 124–131.

[6] Santacesaria, E.; Di Serio, M.; Velotti, R.; Leone, U. Kinetics, mass transfer, and palladium catalyst deactivation in the hydrogenation step of the hydrogen peroxide synthesis via anthraquinone. *Ind. Eng. Chem. Res.* **1994**, *33*, 277–284.

[7] Kosydar, R.; Drelinkiewicz, A.; Ganhy, J. P. Degradation reactions in anthraquinone process of hydrogen peroxide synthesis. *Catal. Lett.* **2010**, *139*, 105–113.

[8] Chen, G. Y.; Liu, J. W.; Li, Q. Q.; Guan, P. F.; Yu, X. F.; Xing, L. S.; Zhang, J.; Che, R. C. A direct H_2O_2 production based on hollow porous carbon sphere-sulfur nanocrystal composites by confinement effect as oxygen reduction electrocatalysts. *Nano Res.* **2019**, *12*, 2614–2622.

[9] Perry, S. C.; Pangotra, D.; Vieira, L.; Csepei, L. I.; Sieber, V.; Wang, L.; de León, C. P.; Walsh, F. C. Electrochemical synthesis of hydrogen peroxide from water and oxygen. *Nat. Rev. Chem.* **2019**, *3*, 442–458.

[10] Jiang, X.; Xiong, Y. X.; Zhao, R. P.; Zhou, J. C.; Lee, J. M.; Tang, Y. W. Trimetallic Au@PdPb nanowires for oxygen reduction reaction. *Nano Res.* **2020**, *13*, 2691–2696.

[11] Wang, Y. L.; Waterhouse, G. I. N.; Shang, L.; Zhang, T. R. Electrocatalytic oxygen reduction to hydrogen peroxide: From homogenous to heterogenous electrocatalysis. *Adv. Energy Mater.* **2020**, 2003323.

[12] Dong, K.; Lei, Y.; Zhao, H. T.; Liang, J.; Ding, P.; Liu, Q.; Xu, Z. Q.; Lu, S. Y.; Li, Q.; Sun, X. P. Noble-metal-free electrocatalysts toward H_2O_2 production. *J. Mater. Chem. A* **2020**, *8*, 23123–23141.

[13] Lu, Z. Y.; Chen, G. X.; Siahrostami, S.; Chen, Z. H.; Liu, K.; Xie, J.; Liao, L.; Wu, T.; Lin, D. C.; Liu, Y. Y. et al. High-efficiency oxygen reduction to hydrogen peroxide catalysed by oxidized carbon materials. *Nat. Catal.* **2018**, *1*, 156–162.

[14] Jung, E.; Shin, H.; Lee, B. H.; Efremov, V.; Lee, S.; Lee, H. S.; Kim, J.; Antink, W. H.; Park, S.; Lee, K. S. et al. Atomic-level tuning of Co-N-C catalyst for high-performance electrochemical H_2O_2 production. *Nat. Mater.* **2020**, *19*, 436–442.

[15] Liu, X.; Liu, H.; Chen, C.; Zou, L. L.; Li, Y.; Zhang, Q.; Yang, B.; Zou, Z. Q.; Yang, H. Fe_2N nanoparticles boosting FeN_x moieties for highly efficient oxygen reduction reaction in Fe-N-C porous catalyst. *Nano Res.* **2019**, *12*, 1651–1657.

[16] Kim, H. W.; Ross, M. B.; Kornienko, N.; Zhang, L.; Guo, J. H.; Yang, P. D.; McCloskey, B. D. Efficient hydrogen peroxide generation using reduced graphene oxide-based oxygen reduction electrocatalysts. *Nat. Catal.* **2018**, *1*, 282–290.

[17] Dong, K.; Liang, J.; Wang, Y. Y.; Xu, Z. Q.; Liu, Q.; Luo, Y. L.; Li, T. S.; Li, L.; Shi, X. F.; Asiri, A. M. et al. Honeycomb carbon nanofibers: A superhydrophilic O_2-entrapping electrocatalyst enables ultrahigh mass activity for the two-electron oxygen reduction reaction. *Angew. Chem., Int. Ed.* in press, DOI: 10.1002/anie.202101880.

[18] Zhang, Q. Z.; Zhou, M. H.; Ren, G. B.; Li, Y. W.; Li, Y. C.; Du, X. D. Highly efficient electrosynthesis of hydrogen peroxide on a superhydrophobic three-phase interface by natural air diffusion. *Nat. Commun.* **2020**, *11*, 1731.

[19] Wang, M. J.; Zhang, N.; Feng, Y. G.; Hu, Z. W.; Shao, Q.; Huang, X. Q. Partially pyrolyzed binary metal-organic framework nanosheets for efficient electrochemical hydrogen peroxide synthesis. *Angew. Chem., Int. Ed.* **2020**, *59*, 14373–14377.

[20] Li, L. Q.; Tang, C.; Zheng, Y.; Xia, B. Q.; Zhou, X. L.; Xu, H. L.; Qiao, S. Z. Tailoring selectivity of electrochemical hydrogen peroxide generation by tunable pyrrolic-nitrogen-carbon. *Adv. Energy Mater.* **2020**, *10*, 2000789.

[21] Wang, Z.; Li, Q. K.; Zhang, C. H.; Cheng, Z. H.; Chen, W. Y.; McHugh, E. A.; Carter, R. A.; Yakobson, B. I.; Tour, J. M. Hydrogen peroxide generation with 100% Faradaic efficiency on metal-free carbon black. *ACS Catal.* **2021**, *11*, 2454–2459.

[22] Xu, Z. Q.; Zhao, H. T.; Liang, J.; Wang, Y.; Li, T. S.; Luo, Y. S.; Shi, X. F.; Lu, S. Y.; Feng, Z. S.; Wu, Q. et al. Noble-metal-free electrospun nanomaterials as electrocatalysts for oxygen reduction reaction. *Mater. Today Phys.* **2020**, *15*, 100280.

[23] Ding, R.; Liu, Y. D.; Rui, Z. Y.; Li, J.; Liu, J. G.; Zou, Z. G. Facile grafting strategy synthesis of single-atom electrocatalyst with enhanced ORR performance. *Nano Res.* **2020**, *13*, 1519–1526.

[24] Cai, H. Z.; Chen, B. B.; Zhang, X.; Deng, Y. C.; Xiao, D. Q.; Ma, D.; Shi, C. Highly active sites of low spin $Fe^{II}N_4$ species: The identification and the ORR performance. *Nano Res.* **2021**, *14*, 122–130.

[25] Ntainjua, N. E.; Piccinini, M.; Pritchard, J. C.; Edwards, J. K.; Carley, A. F.; Moulijn, J. A.; Hutchings, G. J. Effect of halide and acid additives on the direct synthesis of hydrogen peroxide using supported gold-palladium catalysts. *ChemSusChem* **2009**, *2*, 575–580.

[26] Qiang, Z. M.; Chang, J. H.; Huang, C. P. Electrochemical generation of hydrogen peroxide from dissolved oxygen in acidic solutions. *Water Res.* **2002**, *36*, 85–94.

[27] Jirkovský, J. S.; Panas, I.; Ahlberg, E.; Halasa, M.; Romani, S.; Schiffrin, D. J. Single atom hot-spots at Au-Pd nanoalloys for electrocatalytic H_2O_2 production. *J. Am. Chem. Soc.* **2011**, *133*, 19432–19441.

[28] Siahrostami, S.; Verdaguer-Casadevall, A.; Karamad, M.; Deiana, D.; Malacrida, P.; Wickman, B.; Escudero-Escribano, M.; Paoli, E. A.; Frydendal, R.; Hansen, T. W. et al. Enabling direct H_2O_2 production through rational electrocatalyst design. *Nat. Mater.* **2013**, *12*, 1137–1143.

[29] Shen, R. A.; Chen, W. X.; Peng, Q.; Lu, S. Q.; Zheng, L. R.; Cao, X.; Wang, Y.; Zhu, W.; Zhang, J. T.; Zhuang, Z. B. et al. High-concentration single atomic Pt sites on hollow CuS_x for selective O_2 reduction to H_2O_2 in acid solution. *Chem* **2019**, *5*, 2099–2110.

[30] Manzeli, S.; Ovchinnikov, D.; Pasquier, D.; Yazyev, O. V.; Kis, A. 2D transition metal dichalcogenides. *Nat. Rev. Mater.* **2017**, *2*, 17033.

[31] Fu, Q.; Han, J. C.; Wang, X. J.; Xu, P.; Yao, T.; Zhong, J.; Zhong, W. W.; Liu, S. W.; Gao, T. L.; Zhang, Z. H. et al. 2D transition metal dichalcogenides: Design, modulation, and challenges in electrocatalysis. *Adv. Mater.* **2021**, *33*, 1907818.

[32] Zhang, L.; Ji, X. Q.; Ren, X.; Ma, Y. J.; Shi, X. F.; Tian, Z. Q.; Asiri, A. M.; Chen, L.; Tang, B.; Sun, X. P. Electrochemical ammonia synthesis via nitrogen reduction reaction on a MoS_2 catalyst: Theoretical and experimental studies. *Adv. Mater.* **2018**, *30*, 1800191.

[33] Sheng, H. Y.; Hermes, E. D.; Yang, X. H.; Ying, D. W.; Janes, A. N.; Li, W. J.; Schmidt, J. R.; Jin, S. Electrocatalytic production of H_2O_2 by selective oxygen reduction using earth-abundant cobalt pyrite (CoS_2). *ACS Catal.* **2019**, *9*, 8433–8442.

[34] Zhao, X.; Wang, Y.; Da, Y. L.; Wang, X. X.; Wang, T. T.; Xu, M. Q.; He, X. Y.; Zhou, W.; Li, Y. F.; Coleman, J. N. et al. Selective electrochemical production of hydrogen peroxide at zigzag edges of exfoliated molybdenum telluride nanoflakes. *Natl. Sci. Rev.* **2020**, *7*, 1360–1366.

[35] Sheng, H. Y.; Janes, A. N.; Ross, R. D.; Kaiman, D.; Huang, J. Z.; Song, B.; Schmidt, J. R.; Jin, S. Stable and selective electrosynthesis of hydrogen peroxide and the electro-Fenton process on $CoSe_2$ polymorph catalysts. *Energy Environ. Sci.* **2020**, *13*, 4189–4203.

[36] Liang, J.; Wang, Y. Y.; Liu, Q.; Luo, Y. L.; Li, T. S.; Zhao, H. T.; Lu, S. Y.; Zhang, F.; Asiri, A. M.; Liu, F. G. et al. Electrocatalytic hydrogen peroxide production in acidic media enabled by NiS_2 nanosheets. *J. Mater. Chem. A* **2021**, *9*, 6117–6122.

[37] Gerber, I. C.; Serp, P. A theory/experience description of support effects in carbon-supported catalysts. *Chem. Rev.* **2020**, *120*, 1250–1349.

[38] Chen, Y. M.; Li, X. Y.; Park, K.; Zhou, L. M.; Huang, H. T.; Mai, Y. W.; Goodenough, J. B. Hollow nanotubes of N-doped carbon on CoS. *Angew. Chem., Int. Ed.* **2016**, *55*, 15831–15834.

[39] Zhang, C. H.; Fu, L.; Liu, N.; Liu, M. H.; Wang, Y. Y.; Liu, Z. F. Synthesis of nitrogen-doped graphene using embedded carbon and nitrogen sources. *Adv. Mater.* **2011**, *23*, 1020–1024.

[40] Xia, W.; Zhu, J. H.; Guo, W. H.; An, L.; Xia, D. G.; Zou, R. Q. Well-defined carbon polyhedrons prepared from nano metal-organic frameworks for oxygen reduction. *J. Mater. Chem. A* **2014**, *2*, 11606–11613.

[41] Kong, D. S.; Wang, H. T.; Lu, Z. Y.; Cui, Y. $CoSe_2$ nanoparticles grown on carbon fiber paper: An efficient and stable electrocatalyst for hydrogen evolution reaction. *J. Am. Chem. Soc.* **2014**, *136*, 4897–4900.

[42] Xiao, H. Q.; Wang, S. T.; Wang, C.; Li, Y. Y.; Zhang, H. R.; Wang, Z. J.; Zhou, Y.; An, C. H.; Zhang, J. Lamellar structured $CoSe_2$ nanosheets directly arrayed on Ti plate as an efficient electrochemical catalyst for hydrogen evolution. *Electrochim. Acta* **2016**, *217*, 156–162.

[43] Liu, T. T.; Ma, X.; Liu, D. N.; Hao, S.; Du, G.; Ma, Y. J.; Asiri, A. M.; Sun, X. P.; Chen, L. Mn doping of CoP nanosheets array: An efficient electrocatalyst for hydrogen evolution reaction with enhanced activity at all pH values. *ACS Catal.* **2017**, *7*, 98–102.

[44] Liu, T. T.; Asiri, A. M.; Sun, X. P. Electrodeposited Co-doped $NiSe_2$ nanoparticles film: A good electrocatalyst for efficient water splitting. *Nanoscale* **2016**, *8*, 3911–3915.

[45] Li, J.; Liu, G. Y.; Liu, B. B.; Min, Z. Y.; Qian, D.; Jiang, J. B.; Li, J. H. Fe-doped $CoSe_2$ nanoparticles encapsulated in N-doped bamboo-like carbon nanotubes as an efficient electrocatalyst for oxygen evolution reaction. *Electrochim. Acta* **2018**, *265*, 577–585.

[46] Liu, Q.; Tian, J. Q.; Cui, W.; Jiang, P.; Cheng, N. Y.; Asiri, A. M.; Sun, X. P. Carbon nanotubes decorated with CoP nanocrystals: A highly active non-noble-metal nanohybrid electrocatalyst for hydrogen evolution. *Angew. Chem., Int. Ed.* **2014**, *53*, 6710–6714.

[47] Ren, X. P.; Wei, Q. B.; Wu, F.; Wang, Y. H.; Zhao, L. J. CNT/VS_2-MoS_2 with multi-interface structure for improved hydrogen evolution reaction. *Chem. Commun.* **2021**, *57*, 2531–2534.

[48] Wang, Y. J.; Zhao, N. N.; Fang, B. Z.; Li, H.; Bi, X. T.; Wang, H. J. Carbon-supported Pt-based alloy electrocatalysts for the oxygen reduction reaction in polymer electrolyte membrane fuel cells: Particle size, shape, and composition manipulation and their impact to activity. *Chem. Rev.* **2015**, *115*, 3433–3467.